INTERNATIONAL JOURNAL OF ENERGY STUDIES

e-ISSN: 2717-7513 (ONLINE); homepage: https://dergipark.org.tr/en/pub/ijes

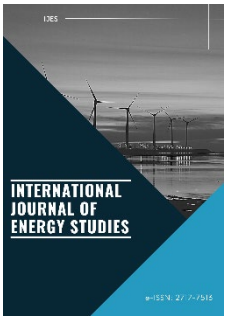

Research Article
Int J Energy Studies 2025; 10(1): 1073-1102
DOI:10.58559/ijes.1591925

Received : 27 Nov 2024
Revised : 31 Dec 2024
Accepted : 11 Jan 2025

Fabrication and characterization of Ni-based electrodes for improved NiZn battery performance

Gizem Cihanoğlu*
Department of Chemical Engineering, İzmir Institute of Technology, 35430 Urla, Türkiye, ORCID: 0000-0002-1524-7634
*(*Corresponding Author:payergizem@gmail.com)*

Highlights

- β-phase nickel hydroxide as a cathode material is synthesized via a traditional hydrothermal method under various conditions.
- The optimized Ni-based electrode has a high current density of 220 mA cm^{-2}.
- NiCoZn composite material is developed for Ni-based electrodes in NiZn batteries.
- NiCoZn electrode in NiZn battery shows excellent capacity of 192.7 mAh g_{active}^{-1}.

You can cite this article as: Cihanoğlu G. Fabrication and characterization of Ni-based electrodes for improved NiZn battery performance. Int J Energy Studies 2025;10(1): 1073-1102.

ABSTRACT

In this study, a hydrothermal method was used to synthesize nickel hydroxide ($Ni(OH)_2$) powders, which are active materials for use in nickel (Ni) electrodes located in nickel-zinc (NiZn) batteries. X-ray diffraction (XRD), scanning electron microscopy (SEM), zeta potential, Brunauer-Emmett-Teller (BET), and electrochemical characterization were used to characterize the cathode material in the prepared Ni electrodes. These results showed a β-phase $Ni(OH)_2$ nanosphere with a well-crystalline structure. The electrochemical test results indicated the Ni electrode has a stable cyclic cycle in the half-cell. Based on the electrochemical performance results, the Ni electrode with $Ni(OH)_2$, which was synthesized at 70°C for 3h of aging time (Ni_pH 12_3h_70°C), was the best-performing metal oxide. Compared with nickel electrodes, the NiCoZn electrode exhibited high OER (oxygen evolution reaction) and ORR (oxygen reduction reaction) activities because the combination of cobalt and zinc oxides with nickel provides excellent electrolyte access capability and promotes effective ion transfer through the active material. The NiZn battery with NiCoZn electrode showed a high capacity of 192.7 mAh g_{active}^{-1} at 10 mA cm^{-2} and cycling durability (after cycling at 10 mA cm^{-2} for 70 cycles). Benefiting from the excellent interaction between Ni, Co, and Zn, NiCoZn exhibited high onset potential and current density, suggesting that the NiCoZn electrode is a promising candidate as a high-performance configuration for Ni-based electrodes in NiZn batteries.

Keywords: Nickel hydroxide synthesis, Nickel electrode, NiZn batteries, Battery performance

1. INTRODUCTION

Recently, interest in alkaline batteries has gained great attention due to their higher specific energy and the high demand for electric vehicles and portable electronic devices [1]. Among alkaline storage batteries, nickel-zinc (NiZn) batteries have been regarded as a promising candidate for energy storage systems due to their theoretical energy density (372 Wh kg^{-1}), high open circuit voltage (1.75 V), low cost, and availability of materials in nature [2, 3]. NiZn batteries exhibit moderate performance with a power density of 140-200 W kg^{-1} and an energy density of 55-85 Wh kg^{-1} when compared to that of other rechargeable Ni-based batteries (NiCd, NiMH, NiFe batteries, etc.) [2, 4].

Nickel hydroxide ($Ni(OH)_2$) has gained much interest in Ni-based alkaline batteries due to its structure, high theoretical capacity, and excellent durability in alkaline electrolytes [5]. $Ni(OH)_2$ possesses a hexagonal layered structure with α and β phases. While α-$Ni(OH)_2$ with an isostructural structure has stacked $Ni(OH)_{2-x}$ layers intercalated with different anions or water molecules, β-$Ni(OH)_2$ with a brucite-like structure contains stacked layers without intercalated species [6, 7]. α-$Ni(OH)_2$ has higher theoretical specific capacity (433 mAh g^{-1}) than that of β-$Ni(OH)_2$ (289 mAh g^{-1}). However, β-$Ni(OH)_2$ is widely used in rechargeable batteries since α-phase is very unstable in water and alkaline media.

In a charge/discharge cycle, β-$Ni(OH)_2$ is converted to β-NiOOH and the α-phase immediately changes to γ-NiOOH, resulting in the swelling of electrode volume by absorbing the alkaline electrolyte due to the high expansion of the γ-phase, leading to reduce discharge potential [8-12].

NiZn batteries have the main challenges for large-scale battery applications such as Zn electrode shape change during the charge/discharge cycles and irreversibility of Ni electrodes [7, 13, 14]. An available approach is to eliminate the swelling of Ni electrodes during the charge/discharge cycles. The swelling phenomenon occurs when β-$Ni(OH)_2$ phase converts into γ-NiOOH, leading to high volume change and rapid capacity loss during charge/discharge cycles [15]. Many studies have been carried out to minimize the swelling phenomenon when increasing the number of charge/discharge cycles. Another effective one is to construct well-defined Ni-based nanostructures as electrodes. It is established that $Ni(OH)_2$ particles and $Ni(OH)_2$ composites with various morphologies such as flowerlike [16], nanotubes [17], nanorods [18], mesoporous films [19], nanosheets [20], spheres [21-23], nanoribbons [24], and stacks of pancakes [25] can be

synthesized by using different methods such as chemical precipitation [26, 27], hydrothermal [28], solvothermal [29, 30], sonochemical [31] and electrodeposition methods [32].

There are several studies in the literature on the synthesis of $Ni(OH)_2$ with good crystallinity, uniformity, high surface area, and uniform particle size distribution to aid the higher electrochemical performance of Ni-based electrodes. Liu and co-workers examined the electrochemical performance of Ni-based electrodes with prepared $Ni(OH)_2$. It was reported that the nickel electrode with 10% nano-sized $Ni(OH)_2$ addition showed higher electrochemical performance compared to the common micro-sized Ni-based electrode [33].

In addition to the change in the morphology and crystallinity of $Ni(OH)_2$, by using active materials, it would be possible to improve the performance and stability of the capacity of Ni electrode during charge/discharge cycles due to providing improved mass transfer kinetics in an alkaline electrolyte and reactions of transition metal ions including OH^- [34]. It is widely known that $Ni(OH)_2$ has poor conductivity because of its semi-conductive nature [35]. The effective approaches to improve these issues have been studied such as the use of various additives, such as bismuth [36], ytterbium [37], yttrium [38], cobalt [33, 35, 39-41], zinc oxide [42], cadmium oxide [43, 44], etc., in Ni-based electrode due to inhibiting the γ-NiOOH formation by altering interlayer bonding forces of the nickel crystal lattice. Cobalt is considered a promising candidate as an additive in the area of Ni-based batteries, to provide an enhancement of nickel electrode conductivity, a better rechargeable by increasing the potential for OER, and/or reducing the Ni electrode working electrode potential, an enhancement of nickel electrode mechanical resistance, and a reduction of γ-NiOOH growth at the Ni electrode during charging that leads to swell and blister the Ni electrode [35, 39, 45]. There are various studies to focus on the inclusion of cobalt as an additive to Ni-based electrodes. For example, Yuan et al. examined the effect of cobalt powder on the electrochemical characteristics of Ni electrodes with co-precipitated $Ni_{1-x}Zn_x(OH)_2$ [35]. It was reported that the discharge capacity and stability were improved when compared to the absence of cobalt powder. The use of cobalt in the Ni-based electrode was investigated by Armstrong et al. [46]. The results showed that the cobalt addition increases the oxygen over potential and the effect of iron poisoning and promotes the utilization of the nickel species. Mao and coworkers examined the influence of cobalt powders with different diameters on the inner pressure of Ni/MH batteries during the charging process [47]. It was pointed out that the cell with the finest cobalt indicated a decline in inner pressure and a long cycle life. Cobalt was used in the study by Sood and groups to examine

the effect on the electrochemical performance of Ni-based electrodes in lineated electrolytes [48]. It was reported that the addition of cobalt in Ni-based electrodes played an effective role in its performance and lifetime.

Herein, we present an investigation of the synthesis, characterization, and electrochemical properties of $Ni(OH)_2$. We attempt to apply different methods to synthesize $Ni(OH)_2$ and to compare the electrodes based on their particle size and crystallinity. The purpose of this study is to determine the optimum synthesis conditions (temperature, reaction pH, and aging time) of $Ni(OH)_2$ powder to improve the electrochemical performance of Ni-based electrodes. We also compare the electrochemical performances of Ni electrodes fabricated by the synthesized $Ni(OH)_2$ powders. We synthesized NiM oxide (M: Metal; cobalt (Co), or cobalt-zinc (Co-Zn)) powders by the hydrothermal method to investigate the activity of the combination of Co and Zn with Ni. We also report the electrochemical performance of Ni electrodes by combining Co and Zn with Ni in a NiZn battery. Excellent behaviors in terms of high current density at constant voltage and good cycle stability make the nanosphere NiCoZn ($Ni_{0.925}Co_{0.05}Zn_{0.025}(OH)_2$) powders a member of the most attractive and promising candidates for Ni-based electrode materials in NiZn batteries.

2. EXPERIMENTAL

2.1. Synthesis of $Ni(OH)_2$ Powder

Nickel (II) hydroxide powder synthesis was carried out via hydrothermal method under various conditions (pH, temperature, and aging time). 2 M $NiSO_4.6H_2O$ (≥99%, Sigma Aldrich) solution and 4 M NaOH (≥98%, Sigma Aldrich) solution were mixed when adjusting pH (9.5 or 12). To control reaction pH, 10 M NH_4OH (≥99%, Sigma Aldrich) buffer solution was added during the experiment. The reaction temperature was adjusted from 50 to 80°C for optimum precipitation. The solution was aged at a desired reaction temperature from 3h to 24h. The liquid phase was vacuum-filtered and separated from the precipitate. To remove excess ions such as SO_4^{2-}, OH^-, and NH_4^+, the precipitate was washed three times with deionised water. The precipitate was dried at 70°C for 15 hours in a vacuum. To observe the effect of additives, cobalt sulfate ($CoSO_4.7H_2O$, ≥99%, Sigma Aldrich) and zinc sulfate ($ZnSO_4.7H_2O$, ≥99%, Sigma Aldrich) were used during the $Ni(OH)_2$ powder synthesis. Additionally, 2 M $NiSO_4.6H_2O$ solution, 0.03 M $CoSO_4.7H_2O$ solution and/or 0.06 M $ZnSO_4.7H_2O$ solution, and 4 M NaOH (≥98%, Sigma Aldrich) solution were mixed at pH 12 and 70°C. Two different solutions were aged for 3h. The same experimental procedure was carried out for synthesis of NiCo and/or NiCoZn powders. Three different kinds

of mixture powders were prepared which are Ni/Co:95/5 (wt.%) and Ni/Co/Zn:92.5/5/2.5 (wt.%). Synthesized $Ni(OH)_2$ powder samples are denoted as shown in Table 1.

Table 1. Identification of $Ni(OH)_2$ samples synthesized in this study

Sample Code	Temperature (°C)	Aging time (h)	pH
Ni_pH 9.5_3h_50°C	50	3	9.5
Ni_pH12_3h_50°C	50	3	12
Ni_pH12_3h_60°C	60	3	12
Ni_pH12_3h_70°C (Ni[a])	70	3	12
Ni_pH12_3h_80°C	80	3	12
Ni_pH12_6h_70°C	70	6	12
Ni_pH12_12h_70°C	70	12	12
Ni_pH12_24h_70°C	70	24	12
NiCo[b]	70	3	12
NiCoZn[c]	70	3	12

a: Ni:100 (wt.%), b: Ni/Co:95/5 (wt.%), c: Ni/Co/Zn:92.5/5/2.5 (wt.%)

2.2. Nickel Electrode Preparation

A 1 cm x 1 cm piece of nickel foam (Nanografi A.S.) as a substrate was used as a current collector. To prepare the pasted nickel electrodes, 85 wt.% as-prepared $Ni(OH)_2$ or NiM (M: Metal, Co or CoZn) hydroxide, 10 wt.% carbon black (Ogan Ocali, A.S.) were used and mixed with a certain amount of 5 wt.% carboxymethyl cellulose (Ogan Ocali, A.S.) solution to obtain a homogeneous paste. The electrode paste was mixed mechanically for about 5 min. The paste was poured into a nickel foam. It was dried at 80 °C for 4 h. Finally, the electrodes were pressed at 10 MPa for 5 min using a hydraulic press (Erdes HP2 hydraulic press) to provide high electrical contact between the nickel foam and the synthesized active materials.

2.3. Characterization

The structures of synthesized $Ni(OH)_2$ powders were determined by X-ray diffraction (XRD) analysis using a Phillips™ Xpert diffractometer. Data was collected from 5-90° in the 2θ range at variable speed (0.336 sec^{-1}). The surface morphology and element distribution of powders in Ni electrodes was studied with Scanning Electron Microscopy (SEM, FEI Quanta250) with energy-dispersive X-ray spectroscope (EDS). Brunauer-Emmett-Teller (BET) analysis (Quantachrome Autosorb) using a nitrogen adsorption/desorption process at 67 K was performed to determine the

surface area and pore size distribution of each sample. A NanoPlus zeta/nanoparticle analyzer was used to investigate the zeta potential and size distribution of each sample which was dispersed in deionized water. To measure the tap density of $Ni(OH)_2$ samples, samples were loaded into a cylinder and tapped 10 times. The weight of the empty cylinder, the powder-filled cylinder, and the volume of $Ni(OH)_2$ were recorded. Therefore, the tap density was determined as follows: powder mass divided by the volume of the cylinder occupied by the powder. Elemental analysis of the amount of Ni, Co and Zn in NiCo and NiCoZn powders was determined from inductively coupled plasma-optical emission spectroscopy (ICP-OES, Agilent 5110).

2.4. Electrochemical Measurements

Electrochemical performance was measured by using a three-electrode potentiostat/galvanostat/ZRA (Gamry model 22162). During electrochemical measurements, a 3-electrode cell with an as-prepared Ni electrode as a working electrode, a Pt wire as the counter electrode, and Ag//AgCl as a reference electrode were used, as shown in Figure 1(a).

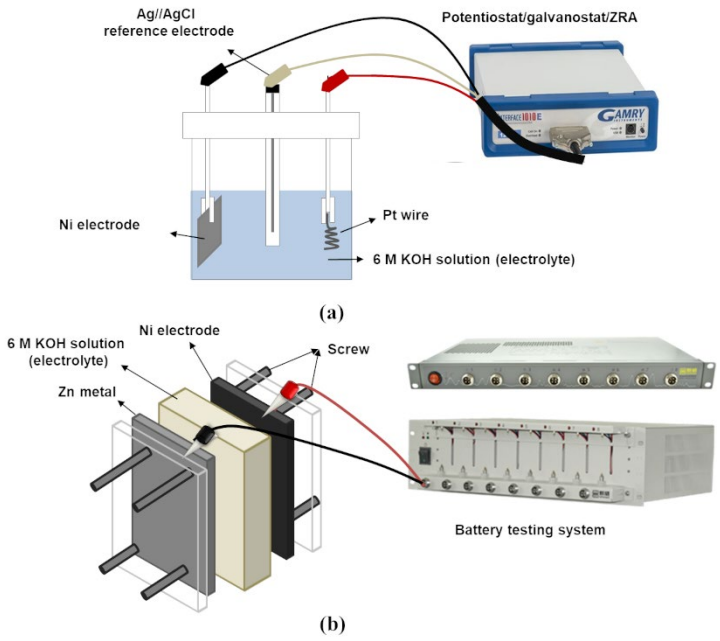

Figure 1. Schematic illustration for (a) half cell (b) full cell experimental set up.

The electrochemical behavior of $Ni(OH)_2$ was studied by cycling voltammetry (CV) and linear sweep voltammetry (LSV) between 0 and 0.8 V at a scan rate of 10 mVs^{-1} in 6M KOH as an electrolyte at 25 ± 2 °C. The NiZn batteries were constructed using a zinc metal plate and a 6 M KOH electrolyte with an excess weight of zinc utilized at the anode. Long-term cycling of the

NiZn battery was accomplished on a battery testing system (NEWARE, CT-4008Tn-5V6A-S1, China), as seen in Figure 1 (b). The NiZn battery was cycled using a constant current/constant voltage (CCCV) charging process at a charge/discharge current of 10/20 mA cm^{-2}.

3. RESULTS AND DISCUSSION

3.1. Characterization of Synthesized $Ni(OH)_2$

Figure 2 shows the influence of synthesis conditions (reaction pH, temperature, and aging time) on the crystallinity of the $Ni(OH)_2$, as revealed by the XRD patterns. The characteristic peaks were consistent with both two known phases, β-$Ni(OH)_2$ and α-$Ni(OH)_2$. This observation indicated that these samples had typically non pure phases [11, 33, 49, 50]. XRD peaks corresponding to (001), (100), (101), (110), (111), (200), (201), (202), and (210) planes of $Ni(OH)_2$ were given at 2θ values of 19.3º, 33.1º, 38.6º, 59.1º, 62.8º, 69.4º, 72.8º, 82.7º and 52.8º, respectively, confirming with the standard values (JCPDS file no.14-0117 and 380715). As shown in Figures 2 (a-c), the difference in diffraction intensity between the samples is ascribed to the presence of their difference in microstructure and morphology. The peaks of (001) and (101) were broadened in samples of Ni_pH 9.5_3h_50ºC and Ni_pH12_3h_50ºC, meaning that there is microdistortion in their structures and the reduction of their crystallite sizes. The control of the crystallinity and chemical structure (morphology, degree of crystallinity, crystalline disorder, crystallite size and crystal growth orientation, etc.) by variation of the preparation conditions such as pH and temperature etc., has been of great interest in the improvement of the electrochemical performance of nickel hydroxide [51-54]. This has a profound and often unpredictable effect on the reversible charge storage capacity of Ni-based batteries. As seen in Figure 2(a), the peaks corresponding to the XRD pattern of Ni_pH 9.5_3h_50ºC are broader than those of Ni_pH 12_3h_50ºC. This indicates that Ni_pH 9.5_3h_50ºC is poorly crystallized. Increasing the precipitation pH leads to a decrease in the crystallite size and an increase in the degree of ordering and crystallinity. Figure 2(b) shows that the XRD peak of the (101) plane for Ni_pH 12_3h_70ºC was higher intense than the (001) plane, confirming that the growth of microstructures were observed along the (001) plane. The small size of the crystallites and crystal growth orientation can result in the high chemical proton diffusion coefficient, which leads to the excellent electrochemical performance of the Ni-based electrodes.

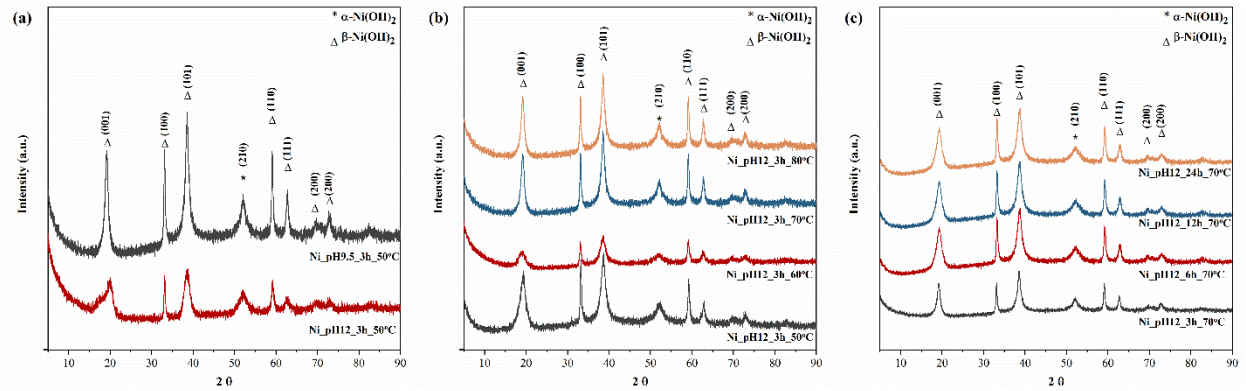

Figure 2. XRD patterns of $Ni(OH)_2$ prepared under different conditions (a) pH (b) temperature (c) aging time.

The synthesis of $Ni(OH)_2$ was confirmed by FTIR results showing the presence of non-hydrogen bonded υO–H vibration groups for β-$Ni(OH)_2$, as seen in Figure 3. High intense stretch at 3642 cm^{-1} shows the presence of non-hydrogen bonded υO–H vibration groups for β-$Ni(OH)_2$ [51]. The broad peak at 3456 cm^{-1} was found to correspond to the hydroxyl groups in α-$Ni(OH)_2$ only for the Ni_pH 9.5_3h_50ºC sample, confirming that they were intercalated water molecules in the interlamellar spaces of $Ni(OH)_2$ in α-phase nickel hydroxide. The sharp and narrow band at 512 cm^{-1} corresponds to the υNi-OH stretching vibration [55-58].

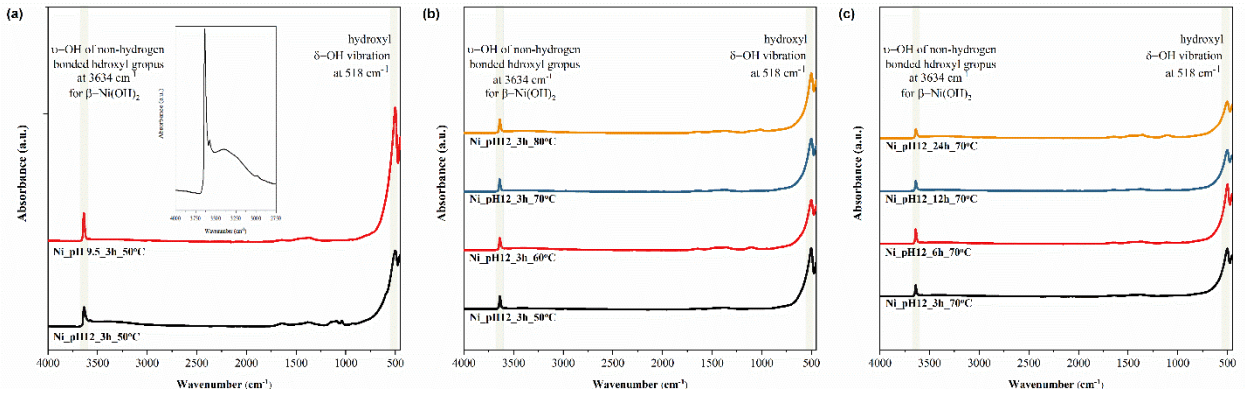

Figure 3. FTIR analysis of all $Ni(OH)_2$ samples.

Figure 4 represents the particle size distribution and zeta potential of all $Ni(OH)_2$ samples. Figures 4(a-c) show the particle size distribution of $Ni(OH)_2$ to understand how operating parameters (reaction pH, temperature, and aging time) affect the particle size of samples. It was found that particle size distribution comparisons were best made for groups of samples derived from different temperatures and aging times. There was a smaller variation in particle size (550-2000 nm) for the Ni_pH9.5_3h_50ºC sample when compared to Ni_pH 12_3h_50ºC. The particle size range of the

Ni_pH12_3h_70ºC sample was found as 1250 nm and 2000 nm. Particle size for Ni_pH12_3h_60 C was distributed in two regions (500-1150 nm and 1150-3500 nm) with low percentage counts (<10%). A similar trend in particle size distribution with temperature change was observed as expected from the zeta potential results. The effect of aging time was found to be due to a difference in the population profile of Ni_pH12_3h_70ºC (1250-2000 nm), Ni_pH12_6h_70ºC (1250-4000 nm), Ni_pH12_12h_70ºC (650-3500 nm) and Ni_pH12_24h_70ºC (550-2500 nm). The reason for this is that the particle size of $Ni(OH)_2$ decreases in case of an increment of aging time. During the aging time as ripening, unstable α-$Ni(OH)_2$ particles gradually dissolve in ammonium solution, leading to the growth of larger β-$Ni(OH)_2$ particles since α-$Ni(OH)_2$ particles with a small number of hydroxyl ions (OH^-) compared to α-$Ni(OH)_2$ particles [59, 60]. The sample of Ni_pH12_3h_70ºC tended to be more organized than the others due to the narrowest population profile. The zeta potential shows the surface charge state of particles in the slurry, implying the type of electrostatic interactions or the control of suspension stability. The traditional tendency of how zeta potential affects the load stability is that zeta potentials higher than +25 mV or lower than −25 mV exhibit well-dispersed, stable, deflocculated particles in slurry [59, 61]. The load stability depends on the region, higher than +30 mV or lower than −30 mV [62]. The results shows that the trends of the zeta potential of $Ni(OH)_2$ changed with process parameters (reaction pH, temperature, and aging time) in ultrapure water at the same pH (8-8.5 of pH), as shown in Figures 4 (d-f). The increase in reaction pH led to an enhancement of the electrostatic charges on the surface of particles. Thus, the sample of Ni_pH12_3h_50ºC was more stable than the sample of Ni_pH9.5_3h_50ºC. Among the $Ni(OH)_2$ samples synthesized at different temperatures, the Ni_pH_12_3h_70ºC showed the maximum surface charge, and its zeta potential was close to -35 mV, as seen in Figure 4 (e). The stability of the load was considered to be excellent. The samples synthesized with various aging times might be considered as moderately stable since the zeta potentials were in the range of -40 to -4 mV (Figure 4 (f)).

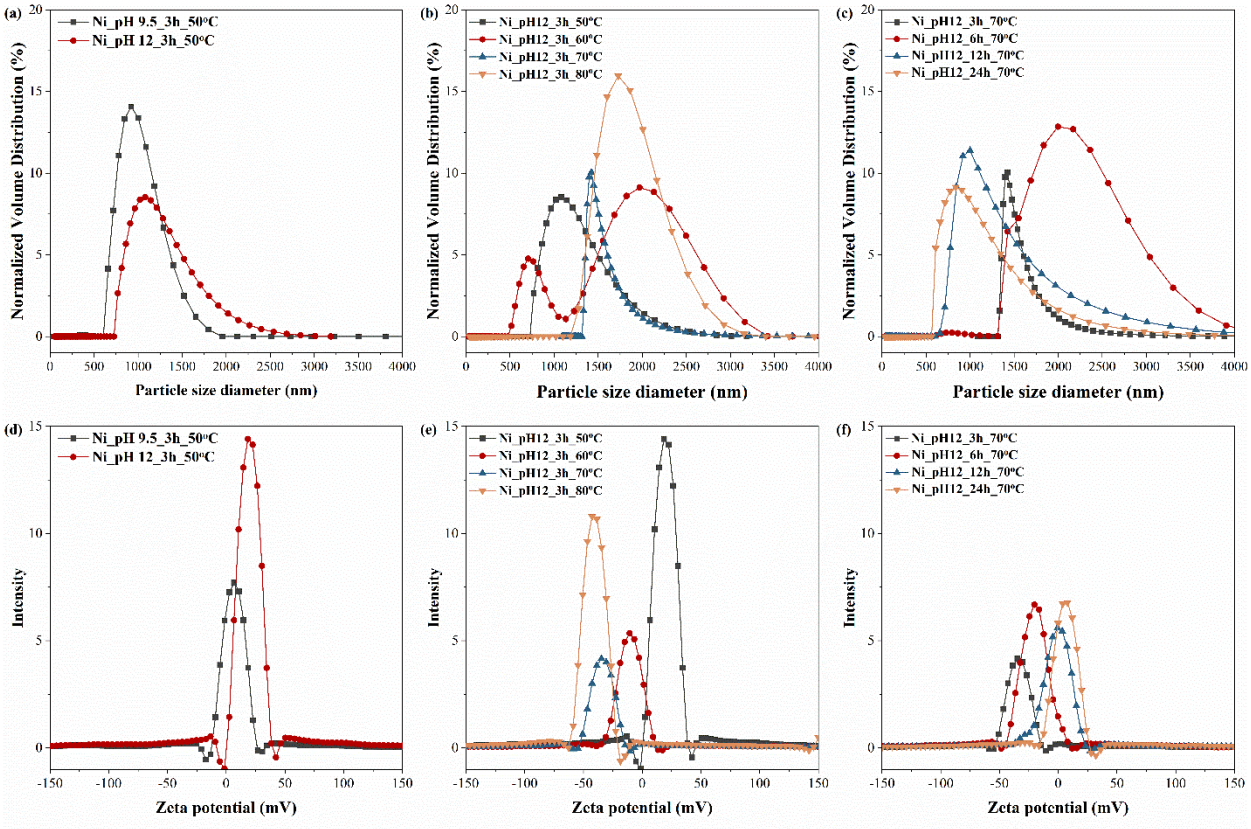

Figure 4. Particle size distribution (a-c) and zeta potential istribution (d-f) of all $Ni(OH)_2$ samples.

We expect that the morphology and surface microstructure of $Ni(OH)_2$ samples play a significant role on the electrochemical performance of NiZn batteries. The nano-particle morphologies of $Ni(OH)_2$ samples synthesized at different conditions (pH, temperature, and aging time) were investigated by SEM, as seen in Figure 5. The Ni_pH9.5_3h_50ºC showed agglomerated nanoparticles with nanosheet stacks. Figure 5 shows that the lower pH led to densely packed layers. The change in reaction pH could directly be related to the crystallinity of $Ni(OH)_2$ polymorphs rather than morphology [25]. The increase in reaction pH led to weaker agglomeration and consisted of lots of finer particles as well as the formation of less organized crystallites. Like the previous study in the literature, nano $Ni(OH)_2$ samples with plate-like shapes were observed when increasing reaction pH (pH>10) [25, 63]. The formation of $Ni(OH)_2$ with a larger spherical shape was obtained at higher reaction temperatures (>50ºC). The grain sizes of samples range from 5 to 35 µm. This observation might be due to the as-synthesized $Ni(OH)_2$ is prevented from growing as the reaction temperature increases [64]. By comparison, the Ni_pH12_3h_70ºC sample exhibited many spherical nanoparticles with well-distributed size having a diameter of 2.5-5 µm (Figure 5 (e)). The effect of aging time on the synthesized $Ni(OH)_2$ morphology was reported in the literature [65]. From Figures 5 (f-i), the products consisted of around 5 µm spherical particles.

The $Ni(OH)_2$ morphologies did not remarkably change with the increase in aging time from 3 h to 24 h, confirming the XRD analysis and particle size distribution results.

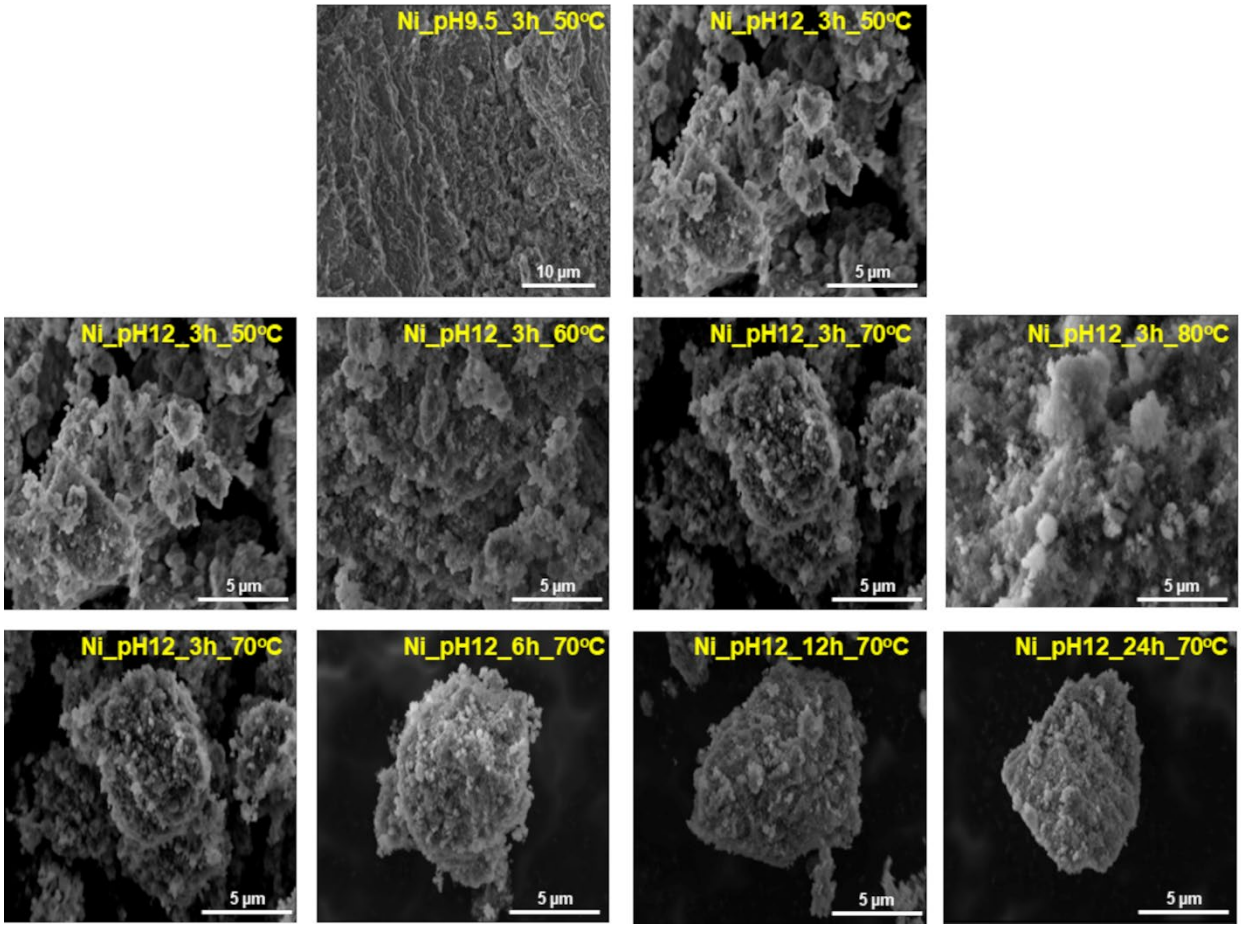

Figure 5. SEM images of all $Ni(OH)_2$ samples synthesized under various conditions.

Nitrogen adsorption-desorption isotherms were performed to examine the structural characteristics, pore size distribution (insets), and surface area of all $Ni(OH)_2$ powders, as shown in Figure 6. All $Ni(OH)_2$ synthesized under different conditions showed the type IV isotherms with H3 hysteresis in the relative pressure (P/P^o) range of 0.005-0.9 according to IUPAC classification, associated with non-rigid aggregates of mesoporous particles that produce slit pores. The behavior of this profile was consistent with capillary condensation in the structures due to the type of pore of solid material [66].

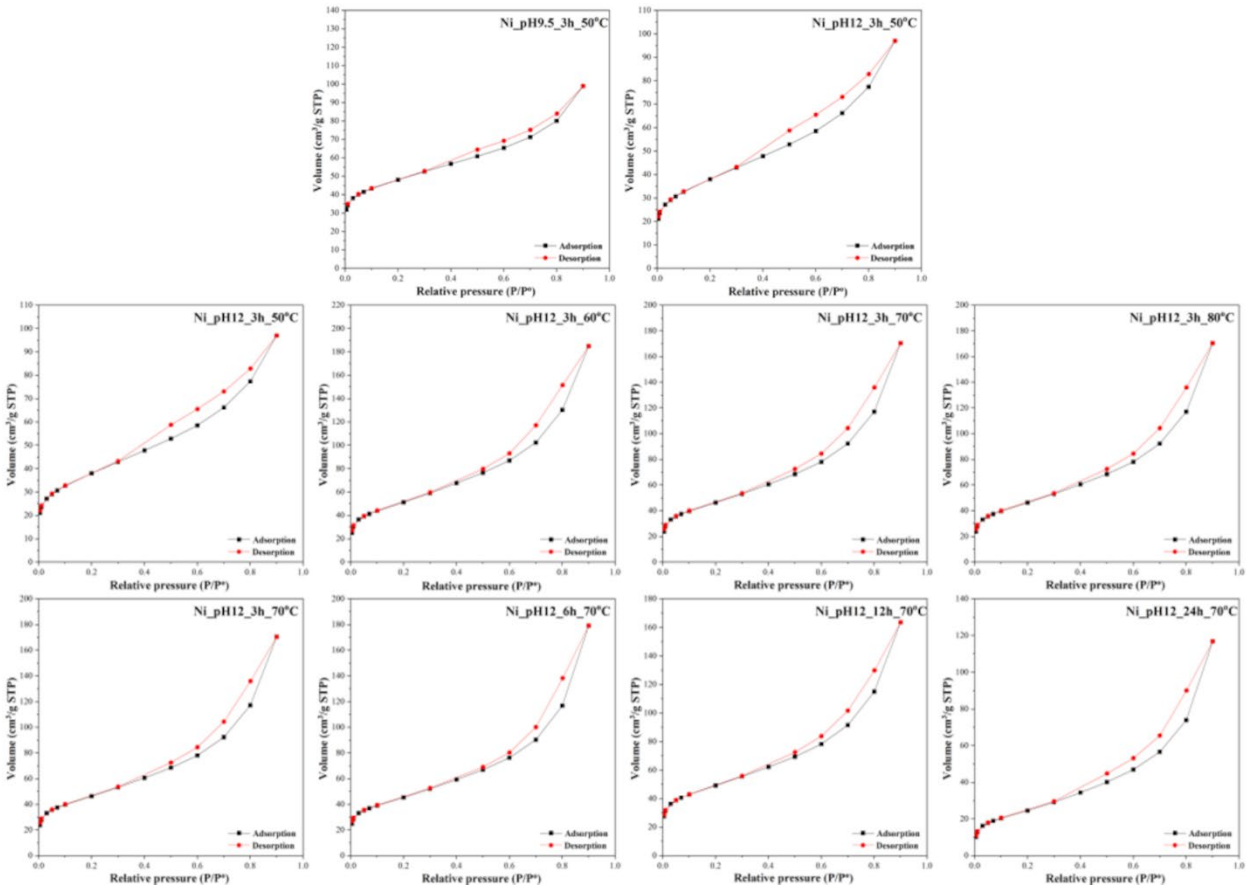

Figure 6. Nitrogen adsorption-desorption isotherms and pore size distribution curve (insets) of all $Ni(OH)_2$ samples.

Table 2 shows pore volume, the BET surface area, and tap density of all $Ni(OH)_2$ samples. The tap density of sample Ni_pH9.5_3h_50ºC was measured to be 0.80 g/cm^3, which was higher than that of Ni_pH12_3h_50ºC (0.56 gcm^{-3}). The reaction temperature improved the tap density varied from 0.56 to 0.8 gcm^{-3}, which might be attributed to the structure of $Ni(OH)_2$ and the formation of agglomeration of particles. Moreover, with increasing aging time from 3 to 24h, the tap density of samples increased from 0.68 to 1.02 gcm^{-3}. The tap densities of the $Ni(OH)_2$ samples in this study were lower when compared with those reported in the literature (2.82 gcm^{-3}) due to their irregular particle morphology and broad particle size distribution [24, 34]. The average pore diameter of these samples was measured to be around 65 Å. All $Ni(OH)_2$ samples presented large BET surface areas and high pore volumes, which might be due to the size of the precursor cations. The results showed that the pore volumes of all samples were in a range of 0.125-0.289 cm^{3}g^{-1}, attributed to surface areas between 132.94 and 178.32 cm^{2}g^{-1} (in Table 2). The Ni_pH12_3h_70ºC sample had the highest surface area (178.32 cm^{2}g^{-1}) and pore volume (0.289 cm^{3}g^{-1}). The effective material

and higher current density have been realized by improving conductivity and reducing polarization via surface modification with $Ni(OH)_2$ samples. Therefore, this observation showed that the Ni_pH12_3h_70ºC sample could be a promising candidate as a material in Ni electrodes for the NiZn battery system due to its better BET surface area and tap density.

Table 2. Tap density, BET surface area, pore diameter, and pore volume and particle size for all $Ni(OH)_2$ samples in different conditions.

	Tap density, g cm^{-3}	**BET specific surface areas, m^2 g^{-1}**	**Average pore diameters, Å**	**Pore volume, cm^3 g^{-1}**	**Particle size, nm**
Ni_pH 9.5	0.80	160.14	45.11	0.131	779.70
Ni_3h_50ºC	0.56	132.94	51.67	0.125	911.23
Ni_3h_60ºC	0.61	183.38	60.26	0.257	1111.50
Ni_3h_70ºC	0.68	184.60	62.31	0.279	1468.62
Ni_3h_80ºC	0.80	133.83	62.24	0.211	1602.85
Ni_3h_70ºC	0.68	184.60	62.31	0.279	1468.62
Ni_6h_70ºC	0.71	160.79	66.28	0.259	1427.16
Ni_12h_70ºC	0.81	178.32	66.19	0.289	844.31
Ni_24h_70ºC	1.02	133.83	62.24	0.211	659.99

3.2. Electrochemical Performance Ni Electrode with Synthesized $Ni(OH)_2$

The electrochemical performance of the as-prepared Ni electrodes was investigated as a function of pH, temperature and aging time. Half-cell oxygen reduction reaction (ORR) and oxygen evolution reaction (OER) CV and LSV comparisons between electrodes with $Ni(OH)_2$ are shown in Figure 7. During the ORR electrochemical activity measurement, the Ni_pH9.5_3h_50ºC electrode exhibited a slightly lower onset potential (E_{onset}) of 31 mV compared with the Ni_pH12_3h_50ºC (32 mV), as seen in Figure 6. Ni_pH12_3h_70ºC electrode showed a high onset potential compared to other samples prepared at different temperatures. This demonstrated that the electrochemical activity of ORR affected the $Ni(OH)_2$ structure properties. Additionally, there was no influence of aging time for $Ni(OH)_2$ synthesis on the electrochemical performance except for 3h aging time.

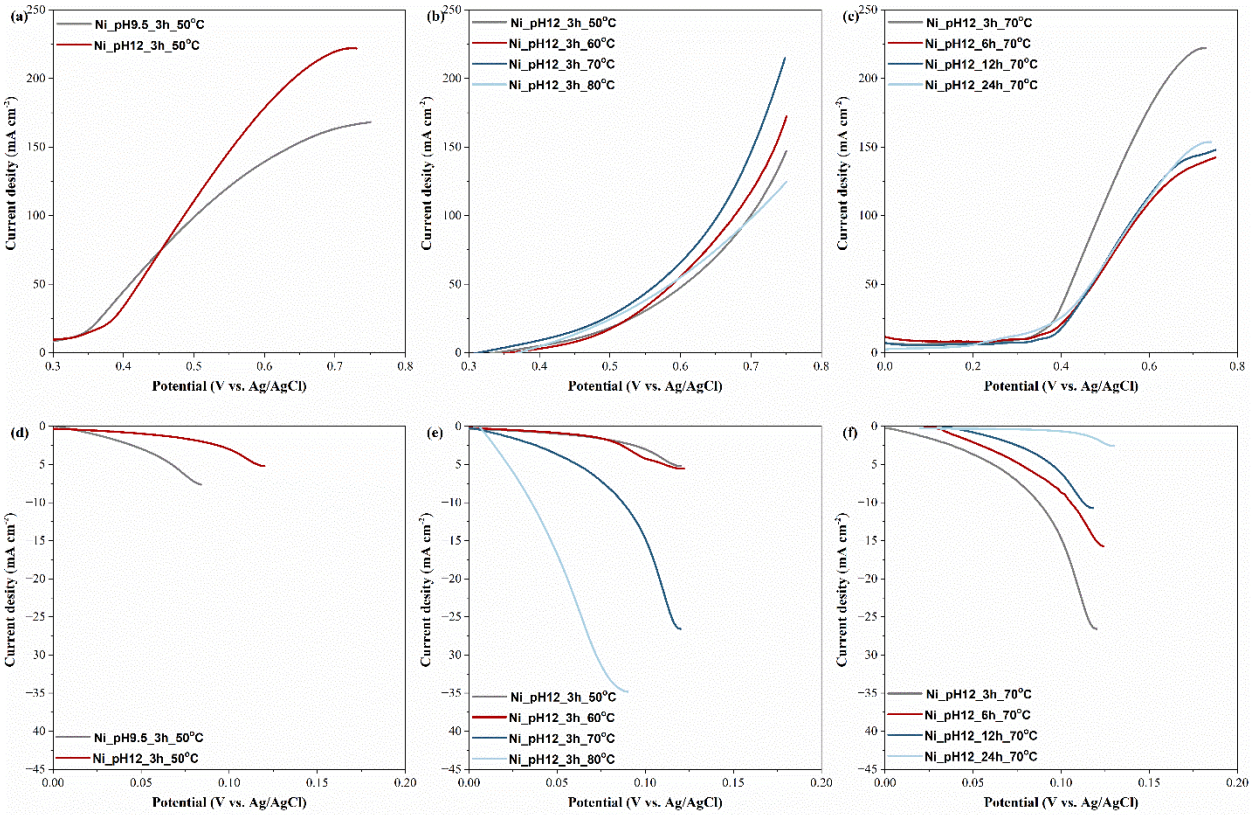

Figure 7. LSV polarization curves measured in 6M KOH of all Ni electrodes for OER and ORR.

During ORR measurements, the Ni_pH12_3h_70ºC electrode exhibited an onset potential of 37 mV which was more positive compared to other Ni electrodes, (see Table 3). Therefore, Ni_pH12_3h_70ºC electrode showed high electrocatalytic activity for ORR. An improvement of electrochemical activity on the Ni_pH12_3h_70ºC electrode was indicated by its slightly smaller E_0 (31 mV) than other Ni electrodes. This might suggest that the spherical nanoparticles of $Ni(OH)_2$ for Ni_pH_12_3h_70ºC showed more electrochemical activity. Therefore, the Ni_pH12_3h_70ºC electrode with high onset potentials and low E_0 is a promising candidate as an electrode material for the NiZn battery system.

Table 3. OER and ORR onset potentials of all Ni electrodes for ORR and OER and E_0

	Onset potential, mV		E_0, mV
	OER	ORR	
Ni_pH 9.5_3h_50°C	32	31	35
Ni_pH 12_3h_50°C	38	32	33
Ni_pH 12_3h_50°C	35	31	32
Ni_pH 12_3h_60°C	28	36	36
Ni_pH 12_3h_70°C	37	37	31
Ni_pH 12_3h_80°C	34	35	34
Ni_pH 12_3h_70°C	37	37	31
Ni_pH 12_6h_70°C	25	30	33
Ni_pH 12_12h_70°C	38	32	34
Ni_pH 12_24h_70°C	16	27	33

The oxidation and reduction peaks of Ni electrodes curves at various reaction conditions were observed in cyclic voltammetry (CV), as shown in Figure 8. This observation showed that the CV area changed with the reaction conditions during $Ni(OH)_2$ synthesis, where the maximum value occurs at 70°C during 3h of aging time. This suggests that the excellent electrochemical activity of $Ni(OH)_2$ was found at this condition. The equivalent catalytic behavior in KOH electrolyte for NiOH oxidation on the Ni electrode (Eq. 1) may be as follows:

$$NiOOH + e^- \rightarrow Ni(OH)_2 + OH^- \quad (1)$$

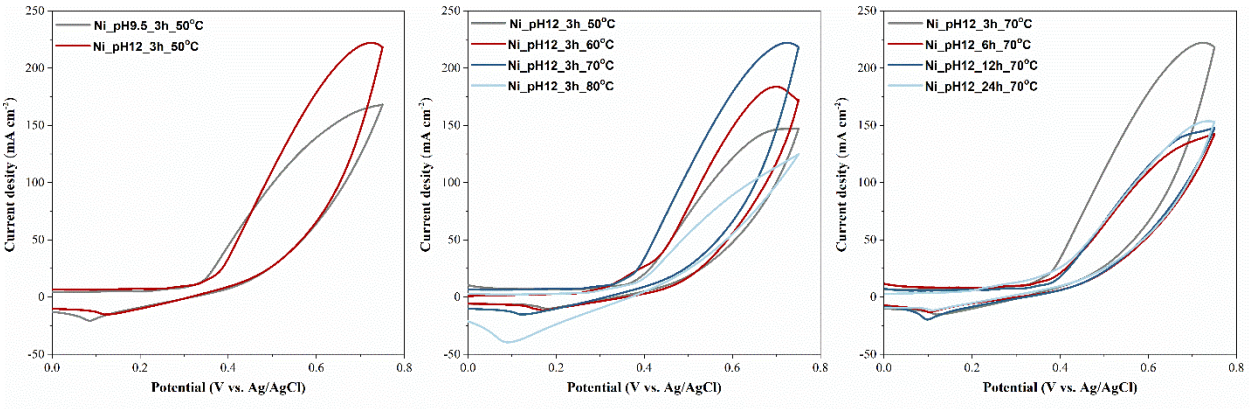

Figure 8. CV curves for measured in 6M KOH of all Ni electrodes with as-fabricated $Ni(OH)_2$.

To understand the electrochemical kinetics of the Ni_pH12_3h_70ºC electrode, its performance parameters were investigated, as seen in Figure 9. The CV curve showed the increase in current densities with the increase in the sweep rate, implying excellent electrochemical performance of the Ni_pH12_3h_70ºC electrode. The peak associated with OER and ORR could be observed over a wide potential range from 0 to 0.8 V. The relationship between current density and scan rate can be calculated using the equation (Eq. 2);

$$\log(j) = \text{blog}(v) + \log(a) \quad (2)$$

where j represents current density, ν is the scan rate. The constant value is represented as a and b is a slope for charge-transfer coefficient. The oxidation and reduction peak current densities for Ni_pH12_3h_70ºC electrodes were found to be $\nu^{0.28}$ and $\nu^{0.62}$, respectively. This observation showed that the reduction and oxidation reactions at the Ni_3h_70ºC electrode are diffusion-controlled processes due to near 0.5 of the "b" value [63].

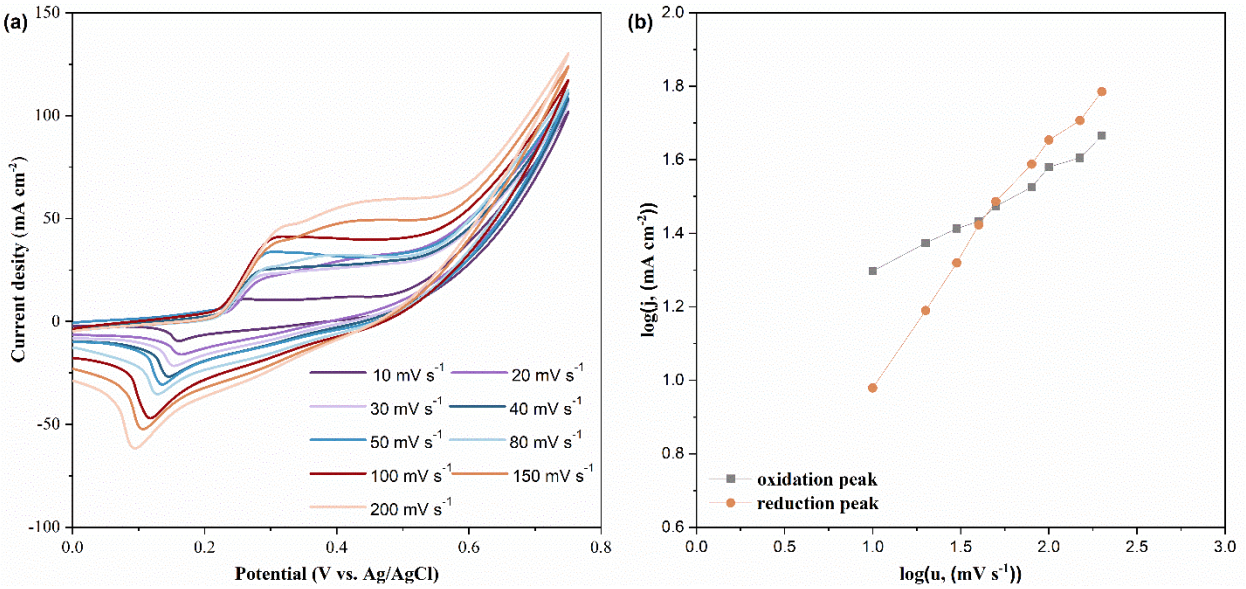

Figure 9. (a) Effect of the voltammetric scan rate on current density for Ni_pH12_3h_70ºC (b) corresponding relation of the logarithm of peak current and the logarithm of the scan rate for OER and ORR.

3.3. Addition of Transition Metals (Co And Zn) as Active Materials for Ni Electrode

There has been considerable interest in transition metals to enhance the performance of Ni-based electrodes due to their cost effectiveness and ready availability [67]. Nickel hydroxides are

employed as an active materials in Ni-based electrodes because nickel in alkaline solution is more conductive to the desorption of OH^-. However, nickel hydroxides usually face critical challenges (limited rate capacity and poor durability) due to weak electrical conductivity and insufficient active sites, leading to hindered ion diffusion [68]. Therefore, studies in the literature focused on the transition metals such as Co, Zn etc. as suitable electrode materials to enhance the electrical conductivity and its active sites [68-71]. Elements such as Al, Cu, Fe, Mn, Sn, Zn and Ca, each of which makes a unique contribution to the electrochemical activity and stability of the cathode, have been used in the search for alternatives to Co. Efforts to find alternatives to Co have led to the use of elements like Zn, Ca, and lanthanides, each contributing uniquely to the cathode's electrochemical activity and stability. The combination of transition (NiCoZn) has garnered significant attention due to their intriguing morphology and structure, indicating improved electrochemical activity. Zinc offers excellent chemical stability, provides to shift the oxygen evolution reaction's overpotential and restricts corrosion resistance, while cobalt provides electrical conductivity, catalytic active sites, and theoretical capacitance [68, 71, 72].

The morphology of NiCo and NiCoZn powders was characterized by scanning electron microscope, and also the elemental analysis was performed using the back-scattering elemental mapping. As depicted in Figure 10, the SEM images of NiCo and NiCoZn illustrate the nano-particle morphologies. There is no significant difference between NiCo and NiCoZn powders due to the low amount of transition metals. As seen in Figure 10(a), the morphology of NiCo is nanoflower spheres with the approximately diameter of 1 μm and particles of are agglomerated and. Figure 10(b) shows that the NiCoZn possesses a wide range of particle size distribution with mixture of spherical and elliptical particles. The EDS analysis confirmed the the synthesis of NiCo and NiCoZn. Figure 10 also shows the presence of Ni, Co and O elements in NiCo and Ni, Co, Zn and O elements in NiCoZn. Moreover, all elements were uniformly distributed in NiCo and NiCoZn. From the mapping analysis, the atomic percentage was identified and NiCo was found to contain 48% Ni, 3% Co and 49% O, while NiCoZn contained 55% Ni, 3% Co, 2% Zn and 40% O. These results suggested that addition of Co and Zn was also confirmed with the synthesis concentration ratio. For comparison to the precursor stoichiometry, the Ni:Co and Ni:Co:Zn ratios measured by EDS analysis were obtained the targeted ratios. This can be attributed to the observation of the expected synthesis of $Ni_{0.95}Co_{0.05}(OH)_2$ and $Ni_{0.925}Co_{0.05}Zn_{0.025}(OH)_2$.

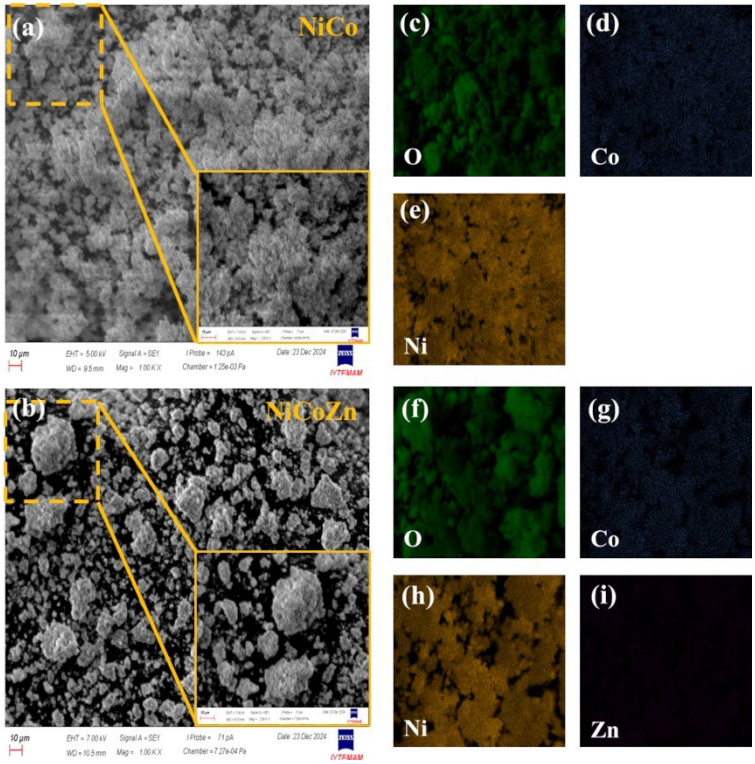

Figure 10. SEM images of (a) NiCo and (b) NiCoZn, EDS results of (c-e) NiCo and (f-i) NiCoZn.

In order to determine the effect of the Co^{2+} and Zn^{2+} substituents on the crystal structure of $Ni(OH)_2$, the crystal structure of NiCo and NiCoZn powders is shown in Figure 11. The diffraction peaks of NiCo ($Ni_{0.95}Co_{0.05}(OH)_2$) and NiCoZn ($Ni_{0.925}Co_{0.05}Zn_{0.025}(OH)_2$) are consistent with the crystalline nature of the β-$Ni(OH)_2$ in the literature, as shown in Figure 11 [68-70]. XRD peaks of β-$Ni(OH)_2$ powder corresponding to (to (001), (100), (101), (102), (110), (111), (103), and (201) planes were obtained at 2θ values of 19.3º, 33.1º, 38.6º, 54.1º, 59.1º, 62.8º, 69.4º, and 72.8º, respectively planes of hexagonal β-$Ni(OH)_2$ (JCPDS:14-0117). The XRD patterns showed that the $Ni(OH)_2$ content was dominant for NiCo and NiCoZn. After addition to Co and Zn, new diffraction peaks do not appear for $Ni_{0.95}Co_{0.05}(OH)_2$ and $Ni_{0.925}Co_{0.05}Zn_{0.025}(OH)_2$, since high content of $Ni(OH)_2$ in the precursors was used the synthesis of NiCo and NiCoZn powders.

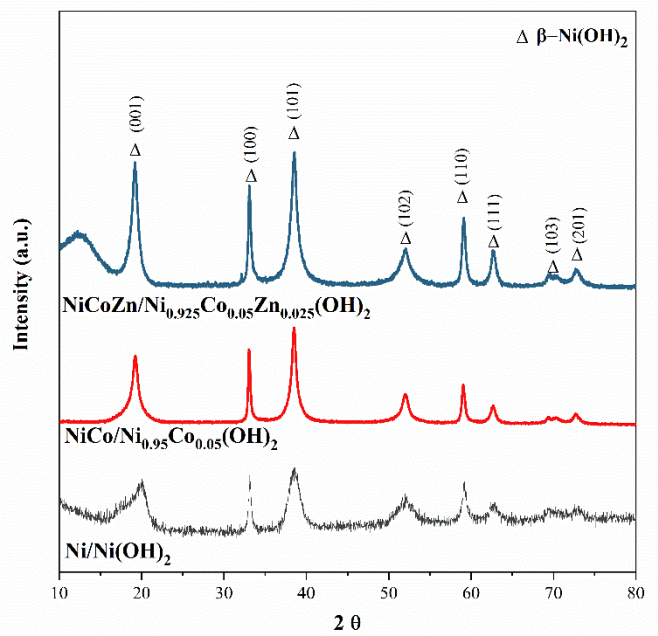

Figure 11. XRD patterns of NiCo and NiCoZn.

ICP-OES analysis is conducted on the cathode materials in Ni-based to determine the amount of metals in the synthesized powders. The Ni:Co and Ni:Co:Zn ratios, $Ni_{0.95}Co_{0.05}$ and $Ni_{0.925}Co_{0.05}Zn_{0.025}$, measured by ICP-OES are the same as the targeted ratios for $Ni_{0.95}Co_{0.05}$ and $Ni_{0.925}Co_{0.05}Zn_{0.025}$ from synthesis, as listed in Table 4. This confirms the content of precursors for NiCo and NiCoZn. The results from ICP_OES analysis confirmed the findings of mapping analysis.

Table 4. Physiochemical characteristics of NiCo and NiCoZn obtained from elemental analysis (ICP-OES)

	Element (wt.%)			Relative weight % from	
	Ni	Co	Zn	synthesis	ICP-OES analysis
NiCo	51.7	2.6		$Ni_{0.95}Co_{0.05}$	$Ni_{0.95}Co_{0.05}$
NiCoZn	55.7	3	1.3	$Ni_{0.925}Co_{0.05}Zn_{0.025}$	$Ni_{0.925}Co_{0.05}Zn_{0.025}$

The effect of transition metals (cobalt and zinc) on the electrochemical performance of the as-prepared Ni electrodes was examined by CV measurements with Ni-based electrodes in contact with the electrolyte (6 M KOH), as shown in Figure 12.

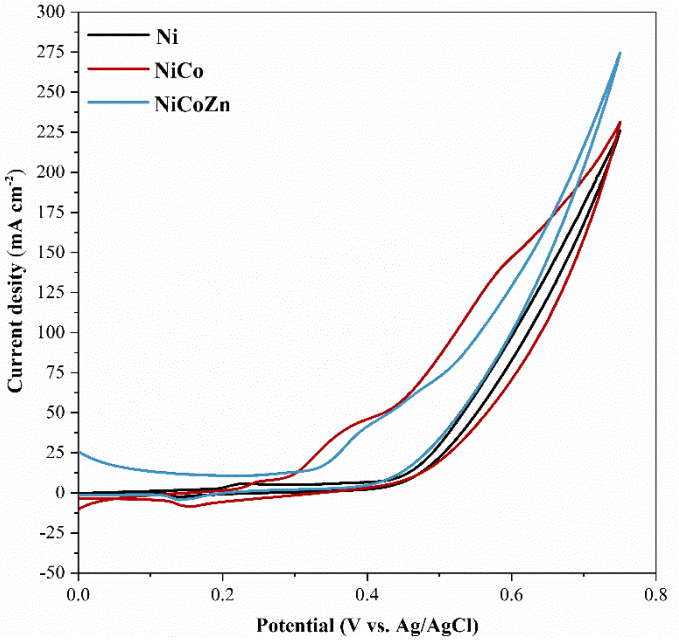

Figure 12. CV curves for measured in 6M KOH of all Ni electrodes with various transition metals.

The redox reaction of Ni based-electrodes takes place due to the reaction of M^{2+} (Ni^{2+}, Co^{2+} and Zn^{2+}) with OH^- [73, 74]. The oxygen evolution mechanism occurs first by adsorption of the hydroxyl group on the electrode. This is followed by the electrochemical desorption of OH^-. Hydrogen peroxide is formed as an intermediate, which decomposes to oxygen. At the same time, the metal and oxygen group bond are broken. The reaction mechanism occurring in alkaline media is shown in Eqs. (3)-(6) (M: metal, Ni, Co, Zn), where M represents an active site and the species adsorption site [75]

$$M{-}OH+OH^- \leftrightarrow M{-}O+H_2O+e^- \quad (3)$$

$$M{-}O+M{-}O \leftrightarrow 2M+O_2 \quad (4)$$

$$M{-}O+OH^- \leftrightarrow M{-}OOH+e^- \quad (5)$$

$$M{-}OOH+OH^- \leftrightarrow O_2+M+H_2O+e^- \quad (6)$$

The overall reaction for the oxidation and reduction peaks (Eq. 7) in CV curves may be as follows:

$$2Ni(OH)_2 + 2Co(OH)_2 + 2Zn(OH)_2 \rightleftharpoons 2NiOOH + 2CoO + 2ZnO + 2H_2O \quad (7)$$

The electrode prepared with NiCoZn showed a higher OER current density (274.7 mA cm^{-2}) when compared to other electrodes. A similar reduction in current density was measured for all Ni

electrodes (Ni, NiCo, and NiCoZn). The higher electrochemical activity measurements for both ORR and OER were observed for the NiCoZn electrode exhibits when compared to Ni and NiCo electrodes due to high onset potential (E_{onset}), as seen in Table 5.

Table 5. OER and ORR onset potentials of Ni electrodes with various transition metals for ORR and OER

	Onset potential, mV	
Electrodes	**OER**	**ORR**
Ni*	63	167
NiCo	162	155
NiCoZn	318	206

*Ni_pH12_3h_50°C

The NiZn batteries with Ni, NiCo and NiCoZn electrodes were tested at a constant current of 10 mA cm^{-2} to examine its electrochemical performance, as seen in Figure 13. The specific capacities of Ni-based electrodes were perfomed by their galvanostatic charge–discharge curves. The specific discharge capacities of 46.7 mAh g_{active}^{-1}, 173.1 mAh g_{active}^{-1} and 192.7 mAh g_{active}^{-1}, were obtained for NiZn batteries with Ni, NiCo and NiCoZn electrodes, respectively. The NiZn battery with NiZnCo exhibited a two-plateau discharge in the 5th cycle (~1.85 V) and delivered the highest discharge capacity (192.7 mAh g_{active}^{-1}) (Figure 13(a)) compared to NiZn batteries with Ni and NiCo electrodes due to potential-energy environments of distinct, reversible Ni-discharge sites. Commercially available NiZn batteries exhibit the specific discharge capacity between 3.5 Ah and 44 Ah [76, 77]. Reported specific discharge capacities of NiZn batteries with Ni-based electrodes such as $NiCo_2O_4$, NiMn/LHD, NiAlCo-LDH/CNT, NiO-CNT//Zn vary between 112 mAh g^{-1} and 184 mAh g^{-1} [78-82].

The charge/discharge cycling stability of the NiZn battery consisting of Ni, Ni Co and NiCoZn electrodes was tested at a current density of 10 mA cm^{-2}, as seen in Figure 13(b). The NiZn battery with NiCoZn electrode showed excellent stability during the charge/discharge cycles. The NiZn batteries with Ni and NiCo electrodes failed after 35th and 55th charge/discharge cycles, respectively. This observation suggests that the NiCoZn electrode is a promising candidate as an electrode with the NiZn battery performance.

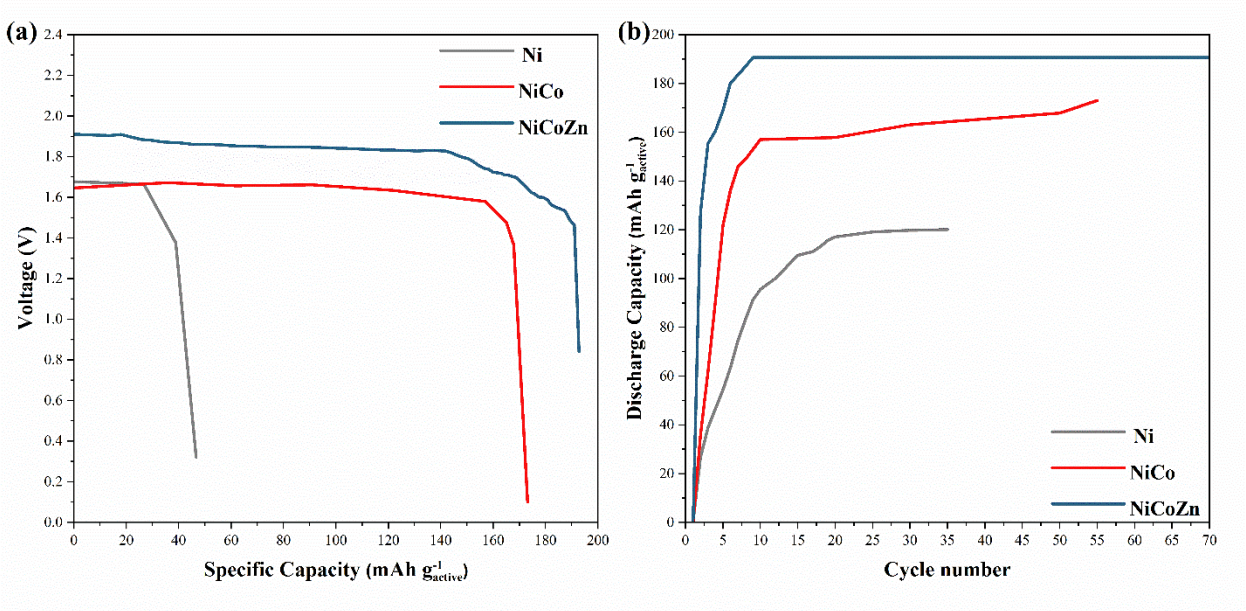

Figure 13. (a) The voltage profiles and (b) discharge capacities vs. time of NiZn batteries with a Ni, NiCo and NiCoZn electrode at 10 mA cm^{-2}.

4. CONCLUSION

This study demonstrated the successful synthesis of $Ni(OH)_2$ with nanosphere structure by a simple hydrothermal method. With the use of Co and Zn as active materials, $Ni_{0.95}Co_{0.05}(OH)_2$ and $Ni_{0.925}Co_{0.05}Zn_{0.025}(OH)_2$ composite materials were synthesized and used as novel electrode materials. The Ni_pH12_3h_50°C (Ni) electrode showed a higher current density of 220 mA cm^{-2} when compared to other as-fabricated Ni electrodes. Combining the enhanced conductivity due to the addition of cobalt and zinc as active materials and the improved ORR and OER performances, the NiCoZn electrode achieved an excellent current density of 374.4 mA cm^{-2}. In addition, we fabricated a promising battery by pairing the NiCoZn electrode with the Zn anode. The NiCoZn powder was tested for NiZn battery application, which presents high discharge capacity and long cycle life in an alkaline electrolyte. It was found that the commercial NiZn batteries exhibited the discharge capacity, varying from 3.5 to 44 Ah [76, 77]. In the literature, the maximum specific discharge capacity (192. 7 mAh g_{active}^{-1}) is much higher than those of NiZn batteries reported such as $NiCo_2O_4$//Zn (183.1 mAh g^{-1}) [78], NiMn/LHD//Zn (180 mAh g^{-1}) [79], NiAlCo-LDH/CNT//Zn (184 mAh g^{-1}) [80], NiO-CNT//Zn (155 mAh g^{-1}) [81], and $NiCo_2O_4$//Zn (112 mAh g^{-1}) [82].The NiZn battery with NiCoZn ($Ni_{0.925}Co_{0.05}Zn_{0.025}$) electrode exhibited a remarkable discharge capacity and good cycling durability (70 cycles), making it a promising candidate for cathode materials in NiZn batteries.

ACKNOWLEDGEMENT

The author would like to thank Prof. Dr. Özgenç EBİL for allowing the use of some of the equipment in his laboratory.

DECLARATION OF ETHICAL STANDARDS

The author of the paper submitted declares that nothing which is necessary for achieving the paper requires ethical committee and/or legal-special permissions.

CONTRIBUTION OF THE AUTHORS

Gizem Cihanoğlu: Performing the experiments and analyzing the results, writing the manuscript.

CONFLICT OF INTEREST

There are no conflicts to declare.

REFERENCES

[1] Shruthi B, Raju VB, Madhu BJ. Synthesis, spectroscopic and electrochemical performance of pasted β- nickel hydroxide electrode in alkaline electrolyte. Spectrochimica Acta Part A: Molecular and Biomolecular Spectroscopy 2015; 135: 683-689.

[2] Jindra J. Progress in sealed Ni-Zn cells, 1991–1995. Journal of Power Sources 1997; 66: 15-25.

[3] Ma M, Tu JP, Yuan YF, Wang XL, Li KF, Mao F, Zeng ZY. Electrochemical performance of ZnO nanoplates as anode materials for Ni/Zn secondary batteries. Journal of Power Sources 2008; 179: 395-400.

[4] Huang H, Zhang L, Zhang WK, Gan YP, Shao H. Preparation and electrochemical properties of ZnO/conductive-ceramic nanocomposite as anode material for Ni/Zn rechargeable battery. Journal of Power Sources 2008; 184: 663-667.

[5] Wiston BR, Ashok M. Electrochemical performance of hydrothermally synthesized flower-like α-nickel hydroxide. Vacuum 2019; 160: 12-17.

[6] Zhao J, Zhang Q. Synthesis of $Ni(OH)_2$ nanoflakes through a novel ion diffusion method controlled by ion exchange membrane and electrochemical supercapacitive properties. Electrochimica Acta 2015; 184: 47-57.

[7] Hu WK, Gao XP, Noréus D, Burchardt T, Nakstad NK. Evaluation of nano-crystal sized α-nickel hydroxide as an electrode material for alkaline rechargeable cells. Journal of Power Sources 2006; 160: 704-710.

[8] Ash B, Mishra KG, Subbaiah T, Paramguru RK, Mishra BK. Electrochemical studies on electrolytic preparation of battery grade nickel hydroxide–Effect of $(OH)^-$ to Ni^{2+} ratio. Journal of Power Sources 2015; 275: 55-63.

[9] Barnard R, Randell CF, Tye FL. Studies concerning charged nickel hydroxide electrodes I. Measurement of reversible potentials. Journal of Applied Electrochemistry 1980;10: 109-125.

[10] Zhou H, Zhou Z. Preparation, structure and electrochemical performances of nanosized cathode active material $Ni(OH)_2$. Solid State Ionics 2005; 176: 1909-1914.

[11] Yang D, Wang R, He M, Zhang J, Liu Z. Ribbon and boardlike nanostructures of nickel hydroxide: synthesis, characterization, and electrochemical properties. The Journal of Physical Chemistry B 2005; 109: 7654-7658.

[12] Barnard R, Crickmore GT, Lee JA, Tye FL. The cause of residual capacity in nickel oxyhydroxide electrodes. Journal of Applied Electrochemistry 1980; 10: 61-70.

[13] Payer G, Ebil Ö. Zinc electrode morphology evolution in high energy density nickel-zinc batteries. Journal of Nanomaterials 2016; 2016: 39.

[14] Oshitani M, Takayama T, Takashima K, Tsuji S. A study on the swelling of a sintered nickel hydroxide electrode. Journal of Applied Electrochemistry 1986; 16: 403-412.

[15] Aladjov B. Battery-grade nickel hydroxide and method for its preparation. U.S. Patent No. 5,788,943. Washington, 1998.

[16] Liu BH, Yu SH, Chen SF, Wu CY. Hexamethylenetetramine directed synthesis and properties of a new family of α-nickel hydroxide organic-inorganic hybrid materials with high chemical stability. The Journal of Physical Chemistry B 2006; 110: 4039-4046.

[17] Cai FS, Zhang GY, Chen J, Gou XL, Liu HK, Dou SX. $Ni(OH)_2$ tubes with mesoscale dimensions as positive-electrode materials of alkaline rechargeable batteries. Angewandte Chemie 2004; 43: 4212-4216.

[18] Matsui K, Kyotani T, Tomita A. Hydrothermal synthesis of single-crystal $Ni(OH)_2$ nanorods in a carbon-coated anodic alumina film. Advanced Materials 2002; 14: 1216-1219.

[19] Tan Y, Srinivasan S, Choi KS. Electrochemical deposition of mesoporous nickel hydroxide films from dilute surfactant solutions. Journal of the American Chemical Society 2005; 127: 3596-3604.

[20] Chen D, Gao L. A new and facile route to ultrafine nanowires, superthin flakes and uniform nanodisks of nickel hydroxide. Chemical Physics Letters 2005; 405: 159-164.

[21] Peng MX, Shen XQ, Wang LS, Wei YH. Structural characteristics of spherical $Ni(OH)_2$ and its charge-discharge process mechanism. Journal of Central South University of Technology 2005; 12: 5-8.

[22] Palanisamy P, Raichur AM. Synthesis of spherical NiO nanoparticles through a novel biosurfactant mediated emulsion technique. Materials Science and Engineering: C 2009; 29: 199-204.

[23] Wang D, Song C, Hu Z, Fu X. Fabrication of hollow spheres and thin films of nickel hydroxide and nickel oxide with hierarchical structures. The Journal of Physical Chemistry B 2005; 109: 1125-1129.

[24] Yang D, Wang R, Zhang J, Liu Z. Synthesis of nickel hydroxide nanoribbons with a new phase: A solution chemistry approach. The Journal of Physical Chemistry B 2004; 108: 7531-7533.

[25] Coudun C, Hochepied JF. Nickel hydroxide "Stacks of Pancakes" obtained by the coupled effect of ammonia and template agent. The Journal of Physical Chemistry B 2005; 109: 6069-6074.

[26] Zhang S, Zeng HC. Self-assembled hollow spheres of β-$Ni(OH)_2$ and their derived nanomaterials. Chemistry Materials 2009; 21: 871-883.

[27] Cao M, He X, Chen J, Hu C. Self-assembled nickel hydroxide three-dimensional nanostructures: A nanomaterial for alkaline rechargeable batteries. Crystal Growth and Design, 2007; 1: 170-174.

[28] Orikasa H, Karoji J, Matsui K, Kyotani T. Crystal formation and growth during the hydrothermal synthesis of β-$Ni(OH)_2$ in one-dimensional nano space. Dalton Transactions 2007; 34: 3757-3762.

[29] Kumari L, Li WZ. Self-assembly of β-$Ni(OH)_2$ nanoflakelets to form hollow submicrospheres by hydrothermal route. Physica E: Low-dimensional Systems and Nanostructures 2009; 41: 1289-1292.

[30] Wang BN, Chen XY, Zhang DW. Controllable synthesis and characterization of CuO, β-$Ni(OH)_2$ and Co_3O_4 nanocrystals in the MCln–NH_4VO_3–NaOH system. Journal of Physics and Chemistry of Solids 2010; 71: 285-289.

[31] Vidotti M, Greco CV, Ponzio EA, Torresi SIC. Sonochemically synthesized $Ni(OH)_2$ and $Co(OH)_2$ nanoparticles and their application in electrochromic electrodes. Electrochemistry Communications 2006; 8: 554-560.

[32] Chou S, Cheng F, Chen J. Electrochemical deposition of $Ni(OH)_2$ and Fe-doped $Ni(OH)_2$ tubes. European Journal of Inorganic Chemistry 2005; 2005: 4035-4039.

[33] Liu X, Yu L. Influence of nanosized $Ni(OH)_2$ addition on the electrochemical performance of Ni(OH)2electrode. Journal of Power Sources 2004; 128: 326–330.

[34] Chen HC, Qin Y, Cao H, Song X, Huang C, Feng H, Zhao XS. Synthesis of amorphous nickel–cobalt–manganese hydroxides for supercapacitor-battery hybrid energy storage system. Energy Storage Materials 2019; 17: 194-203.

[35] Yuan A, Cheng S, Zhang J, Cao C. Effects of metallic cobalt addition on the performance of pasted nickel electrodes. Journal of Power Sources 1999; 77: 178-182.

[36] Pralong V, Delahaye-Vidal A, Beaudoin B, Leriche JB, Tarascon JM. Electrochemical behavior of cobalt hydroxide used as additive in the nickel hydroxide electrode. Journal of the Electrochemical Society 2000; 147: 1306-1313.

[37] He X, Wang L, Li W, Jiang C, Wan C. Ytterbium coating of spherical $Ni(OH)_2$ cathode materials for Ni–MH batteries at elevated temperature. Journal of Power Sources 2006; 158: 1480-1483.

[38] Mi X, Gao XP, Jiang CY, Geng MM, Yan J, Wan CR. High temperature performances of yttrium-doped spherical nickel hydroxide. Electrochimic Acta 2004; 49: 3361-3366.

[39] Ramesh T, Kamath PV. The effect of cobalt on the electrochemical performance of β-nickel hydroxide electrodes. Electrochimica Acta 2008; 53: 8324-8331.

[40] Li X, Dong H, Zhang H. An improvement on redox reversibility of cobalt oxyhydroxide in nickel hydroxide electrodes. Materials Chemistry and Physics 2008; 111: 331-334.

[41] Elumalai P, Vasan HN, Munichandraiah N. Electrochemical studies of cobalt hydroxide-an additive for nickel electrodes. Journal of Power Sources 2001; 93: 201-208.

[42] Tessiera C, Faurea C, Guerlou-Demourgue L, Denagea C, Nabias G, Delmas C. Electrochemical study of zinc-substituted nickel hydroxide. Journal of the Elctrochemical Society 2002; 149: A1136-A1145.

[43] Begum AN, Muralidharan VS, Basha CA. The influences of some additives on electrochemical behaviour of nickel electrodes. International Journal of Hydrogen Energy 2009; 34: 1548-1555.

[44] Oshitani M, Sasaki Y, Takashima K. Development of a nickel electrode having stable performance at various charge and discharge rates over a wide temperature range. Journal of Power Sources 1984; 12: 219-231.

[45] Pralong V, Delahaye-Vidal A, Beaudoin B, Gérand B. Tarascon JM. Oxidation mechanism of cobalt hydroxide to cobalt oxyhydroxide. Journal of Materials Chemistry 1999; 9: 955-960.

[46] Armstrong RD, Briggs GWD, Charles EA. Some effects of the addition of cobalt to the nickel hydroxide electrode. Journal of Applied Electrochemistry 1988; 18: 215-219.

[47] Mao Z, Shan Z, Yin S, Liu B, Wu F. Effect of cobalt powder on the inner pressure of Ni-MH batteries. Journal of Alloys and Compounds 1999; 293-295: 825-828.

[48] Sood AK. Studies on the effect of cobalt addition to the nickel hydroxide electrode. Journal of Applied Electrochemistry 1986; 16: 274-280.

[49] Xiao-Yan G, Jian-Cheng D. Preparation and electrochemical performance of nano-scale nickel hydroxide with different shapes. Materials Letters 2007; 61: 621-625.

[50] Luo Y, Li G, Duan G, Zhang L. One-step synthesis of spherical α-Ni$(OH)_2$ Nanoarchitectures. Nanotechnology 2006; 17: 4278-4283.

[51] Song Q, Tang Z, Guo H, Chan SLI. Structural characteristics of nickel hydroxide synthesized by a chemical precipitation route under different pH values. Journal of Power Sources 2002; 112: 428–434.

[52] Freitas MBJG, Silva e Silva RK, Anjos DM, Rozário A, Manoel PG. Effect of synthesis conditions on characteristics of the precursor material used in NiO·OH/$Ni(OH)_2$ electrodes of alkaline batteries. Journal of Power Sources 2007; 165: 916-921.

[53] Kalam A, Al-Shihri AS, Al-Sehemi AG, Awwad NS, Du G, Ahmad T. Effect of pH on solvothermal synthesis of β-$Ni(OH)_2$ and NiO nano-architectures: Surface area studies, optical properties and adsorption studies. Superlattices and Microstructures 2013; 55: 83-97.

[54] Ramesh TN, Vishnu Kamath P. Synthesis of nickel hydroxide: Effect of precipitation conditions on phase selectivity and structural disorder. Journal of Power Sources 2006; 156: 655-661.

[55] Shangguan E, Chang Z, Tang H, Yuan XZ, Wang H. Synthesis and characterization of high-density non-spherical $Ni(OH)_2$ cathode material for Ni-MH batteries. International Journal of Hydrogen Energy 2010; 35: 9716-9724.

[56] Abbas SA, Iqbal MI, Kim SH, Khan HA, Jung KD. Facile synthesis of alfa-nickel hydroxide by an ultrasound-assisted method and its application in energy storage devices. Applied Surface Science 2019; 474: 218-226.

[57] Kumar NS, Ganapathy M, Sharmila S, Shankar M, Vimalan M, Potheher IV. ZnO/$Ni(OH)_2$ core-shell nanoparticles: Synthesis, optical, electrical and photoacoustic property analysis. Journal of Alloys and Compounds 2017; 703: 624-632.

[58] Liu K, Zhou W, Zhu D, He J, Li J, Tang Z, Huang L, He B, Chen Y. Excellent high-rate capability of micron-sized Co-free α-$Ni(OH)_2$ for high-power Ni-MH battery. Journal of Alloys and Compounds 2018; 768: 269-276.

[59] Andrade TM, Danczuk M, Anaiss FJ. Effect of precipitating agents on the structural, morphological, and colorimetric characteristics of Nickel hydroxide particles. Colloid and Interface Science Communications 2018; 23: 6-13.

[60] Hall DS, Lockwood DJ, Bock C, MacDougall BR. Nickel hydroxides and related materials: a review of their structures, synthesis and properties. Proceedings of the Royal Society A 2015; 471: 1-65.

[61] Vallar S, Houivet D, El Fallah J, Kervadec D, Haussonne JM. Oxide slurries stability and powders dispersion: Optimization with zeta potential and rheological measurements. Journal of European Ceramic Society 1999; 19: 1017-1021.

[62] Porpino KKP, Barreto MCS, Cambuim KB, Carvalho Filho JR, Toscan, IA, Lima MA. Fe (II) adsorption on Ucides cordatus crab shells. Quím. Nova 2011; 34: 928–932.

[63] Palanisamy P, Raichur AM. Synthesis of spherical NiO nanoparticles through a novel biosurfactant mediated emulsion technique. Materials Science and Engineering: C 2009; 29: 199-204.

[64] Gund GS, Dubal DP, Jambure SB, Shinde SS, Lokhande CD. Temperature influence on morphological progress of $Ni(OH)_2$ thin films and its subsequent effect on electrochemical supercapacitive properties. Journal of Materials Chemistry A 2013; 1: 4793-4803.

[65] Parveen N, Cho MH. Self-assembled 3D flower-like nickel hydroxide nanostructures and their supercapacitor applications, Nature Scientific Reports 2016; 6: 1-10.

[66] Mi X, Gao XP, Jiang CY, Geng MM, Yan J, Wan CR. High temperature performances of yttrium-doped spherical nickel hydroxide. Electrochimic Acta 2004; 49: 3361-3366.

[67] Osgood H, Devaguptapu SV, Xu H, Cho J, Wu G. Transition metal (Fe, Co, Ni, and Mn) oxides for oxygen reduction and evolution bifunctional catalysts in alkaline media. Nano Today 2016; 11(5): 601-625.

[68] Du Y, Li G, Zhao L, Ye L, Che C, Liu X, Liu H, Yang X. Core–Shell MnO_2 Nanotubes @Nickel–Cobalt–Zinc hydroxide nanosheets for supercapacitive energy storage. ACS Applied Nano Materials 2020; 3: 8-28.

[69] Kumar AS, Sai KNS, Prasad K, Tighezza AM, Pabba DP, Kim JS, Joo SW. *In-situ* constructed NiCoZnS composite on nickel foam with hierarchical structures as bifunctional electrocatalysts for oxygen evolution reaction (OER) and supercapacitors. Journal of Alloys and Compounds 2024; 1005: 175983.

[70] Durai L, Gopalakrishnan A, Badhulika S. Highly stable NiCoZn ternary mixed-metal-oxide nanorods as a low-cost, non-noble electrocatalyst for methanol electro-oxidation in alkaline medium. Energy & Fuels 2021; 35: 12507-12515.

[71] Yang Z, Zhang Y, Feng C, Wu H, Ding Y, Me H. P doped NiCoZn LDH growth on nickel foam as an highly efficient bifunctional electrocatalyst for overall Urea-Water electrolysis. International Journal of Hydrogen Energy 2021; 46: 25321-25331.

[72] Bello IT, Raza H, Michael AT, Muneeswara M, Tewari N, Bingsen W, Cheung YN, Choi Z, Boles ST. Charging Ahead: The evolution and reliability of Nickel-Zinc battery solutions. EcoMat 2025; 3: 1-36.

[73] Rastgoo-Deylami M, Esfandiar A. High energy aqueous rechargeable nickel-zinc battery employing hierarchical NiV-LDH nanosheet-built microspheres on reduced graphene oxide. ACS Applied Energy Materials 2021; 4: 2377–2387

[74] Wu M, Xia Z, Mao Z, Lu J, Yan J, Li Z, He Y, Liu H, Cheng B. Stretchable Ni-Zn fabric battery based on sewable core-shell SCNF@Ni@NiCo LDHs thread cathode for wearable smart garment. Journal of Materials Science 2021; 56: 10537–10554

[75] Zhang X, Alvarado-Ávila MI, Liu Y, Yu D, Ye F, Dutta J. Self-sacrificial growth of hierarchical P(Ni, Co, Fe) for enhanced asymmetric supercapacitors and oxygen evolution reactions. Electrochimica Acta 2023; 438: 141582.

[76] Zhou W, Zhu D, He J, Li J, Chen H, Chen Y, Chao D. A scalable top-down strategy toward practical metrics of Ni–Zn aqueous batteries with total energy densities of 165 W h kg^{-1} and 506 W h L^{-1}. Energy&Environmental Science, 2020; 13: 4157-4167.

[77] Pavlov AP, Grigorieva LK, Chizhik SP, Stankov VK. Nickel-zinc batteries with long cycle life. Journal of Power Sources 1996; 62:113-116.

[78] Zhang H, Zhang X, Li H, Zhang Y, Zeng Y, Tong Y, Zhang P, Lu X. Flexible rechargeable Ni//Zn battery based on self-supported $NiCo_2O_4$ nanosheets with high power density and good cycling stability. Green Energy & Environment 2018; 3: 56-62.

[79] Wang S, Duan X, Gao T, Wang Z, Zhou D, Sun K, Shang Z, Kuang Y, Tian S, Li X, Liu W, Sun X. Zn doped NiMn-Layered double hydroxide for high performance Ni–Zn Battery. Journal of The Electrochemical Society 2020; 167:160550.

[80] Gong M, Li Y, Zhang H, Zhang B, Zhou W, Feng J, Wang H, Liang Y, Fan Z, Liu J, Dai H. Ultrafast high-capacity NiZn battery with NiAlCo layered double hydroxide. Energy&Environmental Science 2014; **7**: 2025.

[81] Wang X, Li M, Wang Y, Chen B, Zhu Y, Wu Y. A Zn–NiO rechargeable battery with long lifespan and high energy density. Journal of Materials Chemistry A 2015; 3: 8280.

[82] Wang J, Jia Z, Li S, Wang Y, Guo W, Qi T. High-performance aqueous rechargeable batteries based on zinc anode and $NiCo_2O_4$ cathode. Bulletin of Materials Science 2015; 38: 1435-1438.